

PAPER

Orderly hysteresis in field-driven robot swarm active matter

To cite this article: Yanping Liu *et al* 2023 *Chinese Phys. B* **32** 068701

View the [article online](#) for updates and enhancements.

You may also like

- [Angular insensitive nonreciprocal ultrawide band absorption in plasma-embedded photonic crystals designed with improved particle swarm optimization algorithm](#)
Yi-Han Wang, , Hai-Feng Zhang et al.
- [Identifying Influential Spreaders in Social Networks: A Two-Stage Quantum-Behaved Particle Swarm Optimization with Lévy Flight](#)
Pengli Lu, Jimao Lan, Jianxin Tang et al.
- [Bio-inspired environmental adaptability of swarm active matter](#)
Yangkai Jin, Gao Wang, Daming Yuan et al.

Orderly hysteresis in field-driven robot swarm active matter

Yanping Liu(刘艳萍)¹, Gao Wang(王高)^{2,3}, Peilong Wang(王培龙)^{2,4}, Daming Yuan(袁大明)^{2,4}, Shuaxiu Hou(侯帅旭)¹, Yangkai Jin(金阳凯)^{2,4}, Jing Wang(王璟)^{2,3,†}, and Liyu Liu(刘雳宇)^{1,‡}

¹Chongqing Key Laboratory of Soft Condensed Matter Physics and Smart Materials, College of Physics, Chongqing University, Chongqing 401331, China

²Wenzhou Institute, University of Chinese Academy of Sciences, Wenzhou 325011, China

³School of Physical Sciences, University of Chinese Academy of Sciences, Beijing 100049, China

⁴School of Biomedical Engineering, School of Ophthalmology and Optometry, Eye Hospital, Wenzhou Medical University, Wenzhou 325001, China

(Received 27 January 2023; revised manuscript received 3 March 2023; accepted manuscript online 28 March 2023)

Boundary effect and time-reversal symmetry are hot topics in active matter. We present a biology-inspired robot-environment-interaction active matter system with the field-drive motion and the rules of resource search, resource consumption, and resource recovery. In an environmental compression–expansion cycle, the swarm emerges a series of boundary-dependent phase transitions, and the whole evolution process is time-reversal symmetry-breaking; we call this phenomenon “orderly hysteresis”. We present the influence of the environmental recovery rate on the dynamic collective behavior of the swarm.

Keywords: time-reversal symmetry-breaking, phase transitions, robot swarm, active matter

PACS: 87.15.Zg, 89.75.Fb, 05.65.+b, 87.85.St

DOI: 10.1088/1674-1056/acc803

1. Introduction

Active matter, which is a collective name covering many nonequilibrium condensed systems composed of self-driven units or active particles, is highly related to many important physical and biological phenomena, such as self-organization, self-adaption, morphogenesis, collective migration, and so on.^[1–6] A defining key feature of active matter is the fact that each basic component can convert local energy into systematic movement.^[7] In the field of active matter, spatial ordered states such as the nematic and the polar,^[8,9] collective motions such as flocking and active turbulence,^[10–13] and the relation of the interaction of active particles with each other or with the environment to collective motion^[14,15] are hot topics. But due to the complexity, the instability and the uncontrollability of many traditional active matter systems, many questions in active matter are not yet answered.

With the continuous development of robotics, autonomous robots become increasingly smaller, easier to make and more adaptive, and thus set a new trend of combining robotics with physical research^[16–18] or biological research.^[19–23] In our previous work,^[24] we designed a biology-inspired robot swarm active matter system in which the robots can self-modify their local environment and respond to the change of environment, and then a series of collective state changes emerged. This swarm system confirmed the great variety of ordered patterns and transitions in active matter^[25,26] once again. However, some common questions in active matter such as the influence of the environmental boundary shape,^[27–29] the time-reversal symmetry of the

swarm evolution,^[30,31] and the influence of the key environment parameters,^[32] were previously understudied in this system.

In this paper, we studied the influence of an environmental compression–expansion cycle on the robot swarm active matter system with the rules of resource search, resource consumption and resource recovery when the environmental boundary is circular or square. The spatial structure of the swarm is highly dependent on the geometry of the environmental boundary. In the expansion stage the evolution process of the swarm with obviously more fluidity and disorder is far different from it in the compression stage, which indicates a time-reversal symmetry-breaking orderly hysteresis phenomenon in this system.

2. Methods

2.1. Design of the robot-environment-interaction system

The whole biological-ecology-inspired robot swarm active matter system is composed of dozens of mobile robots which can sense the light environment and a light environment platform composed of a light-emitting diode (LED) light board, a camera, and a corresponding computer control system, and able to detect the positions of the robots and adjust local light intensities according to these positions. Each 65-mm-diameter robot is composed of four semiconductor-based RGB (red, green, blue) sensors, two pulse width modulated (PWM) motor-driven wheels, two rechargeable polymer lithium batteries, a processor, a motor driver integrated circuit (IC), three R/G/B LEDs and an infrared (IR) LED in a semi-transparent

[†]Corresponding author. E-mail: wangjing@ucas.ac.cn

[‡]Corresponding author. E-mail: lyliu@cqu.edu.cn

cover, two curved metallic charging hooks, and a series of auxiliary electronics. The four bottom and downward-looking RGB sensors are symmetrically cross-distributed and keep about 3-mm distance from the ground. Each sensor independently detects a local light intensity from a different position underneath, and then transfers the signal to the processor. Combining the four intensity values of the light environment, the processor can calculate the light gradient vectors in two mutually vertical directions and then transfer the advancing direction information to the motor driver IC. Finally, controlled by the two-wheel independent drive system, the robot can move to seek the maximum light intensity in the environment, as shown in Fig. 1(a). Hence, every robot has the ability to search the light resource with velocity v_n ,

$$v_n = \kappa \nabla I(x_n, y_n; t), \quad (1)$$

where (x_n, y_n) is the position of robot n at time t and κ is the robotic motion sensitivity to the local gradient of the two-dimensional (2D) light resource intensity landscape I .

The resource consumption and resource recovery functions are mainly realized by the light environment platform, as

$$\begin{cases} \partial_t I = \frac{1}{\tau_R} (I_0 - I) - \sum_n k_c \exp \left\{ -\frac{[(x-x_n)^2 + (y-y_n)^2]}{2\sigma^2} \right\}, & \text{when } I > 0, \\ \partial_t I = \frac{1}{\tau_R} (I_0 - I), & \text{when } I = 0. \end{cases} \quad (2)$$

Hence, the computer can calculate and generate new light environment images and exports them to the LED light board via the controller. The whole cycle timestep from the image acquisition to the landscape export takes about 0.2 second.

In this robot-environment-interaction system with such resource rules, the robots emerge many novel kinetic characteristics which are summarized as field-drive motion in our previous work.^[24,33] One of the key kinetic characteristics is the symmetry-breaking starting. Under ideal conditions, when there is only one robot or the distance between any two robots is long enough, the local light intensity landscape consumed by a stationary robot is spatially symmetric, so there shall be no nonzero gradient for the robot to move. In other words, the robots have no intrinsic motion on the design level. But in the real experiments, this spatial symmetry is spontaneously broken by electronic noise in the intensity sensors and errors in measurement of robots' positions during image acquisition and processing. After multiple positive-feedback processes, these noises then bootstrap the robot into an emergent directional motion. Consequently, this symmetry-breaking starting makes our robot swarm a typical active matter system. Another counterintuitive behavior of our robots is the counter-gradient motion. There is no doubt that in a

shown in Figs. 1(b) and 1(c). The arena for the robots is the square 3.84 m × 3.84 m LED light board which is also the main part of the light environment with a 1.25-mm pitch. In this study, a quarter of the whole LED light board is chosen as the main experimental area. To acquire the positions of the robots, a high-resolution IR CCD camera is installed right above the center of the experimental area to obtain the information of the signal lamps which are located at the centers of all the robots, and each pixel of the camera matches a pixel of the light board to insure the spatial accuracy of robots' positions. The continuous images are transferred to the computer and real-time image analysis is executed to precisely extract the locations of robots. Combining the robots' positions $\{(x_n, y_n)\}$, the robotic characteristic resource consumption rate k_c , the robotic characteristic resource consumption radius σ , the robot-free original light intensity I_0 , and the environment recovery characteristic time τ_R , the presence of each robot can immediately consume the local light resource in a Gaussian circle around its position and the light resource recovers once the robot goes away, causing the whole light resource landscape to change as

sufficiently strong externally imposed gradient a robot shall move along the global resource gradient. However, when the global resource gradient is weak enough, the motion mode of the robot changes. Because of the local digging of resource holes, an opposite local gradient may emerge, and the robot can move against the global resource gradient. By the theoretical estimation,^[24] the maximum resource slope S_m a robot can move against can be calculated as

$$S_m \approx 0.35 \frac{k_c \tau_R}{\sigma}. \quad (3)$$

This counter-gradient motion makes robots have the ability to escape from local resource peaks or valleys, and then leads to a variety of interesting collective behaviors. Since the resource gradients give the robots motility, the moving robots should immediately stop by the next time step iteration once all the gradients are removed. Therefore, another key property of the field-drive robots is that they have no physical inertia.

2.2. Experimental procedure and analysis methods

Density-dependent phase transitions are a big class of important phenomena in active matter and self-organization phenomenon,^[34] and the environmental compression and expansion are common means to control matter density. In our

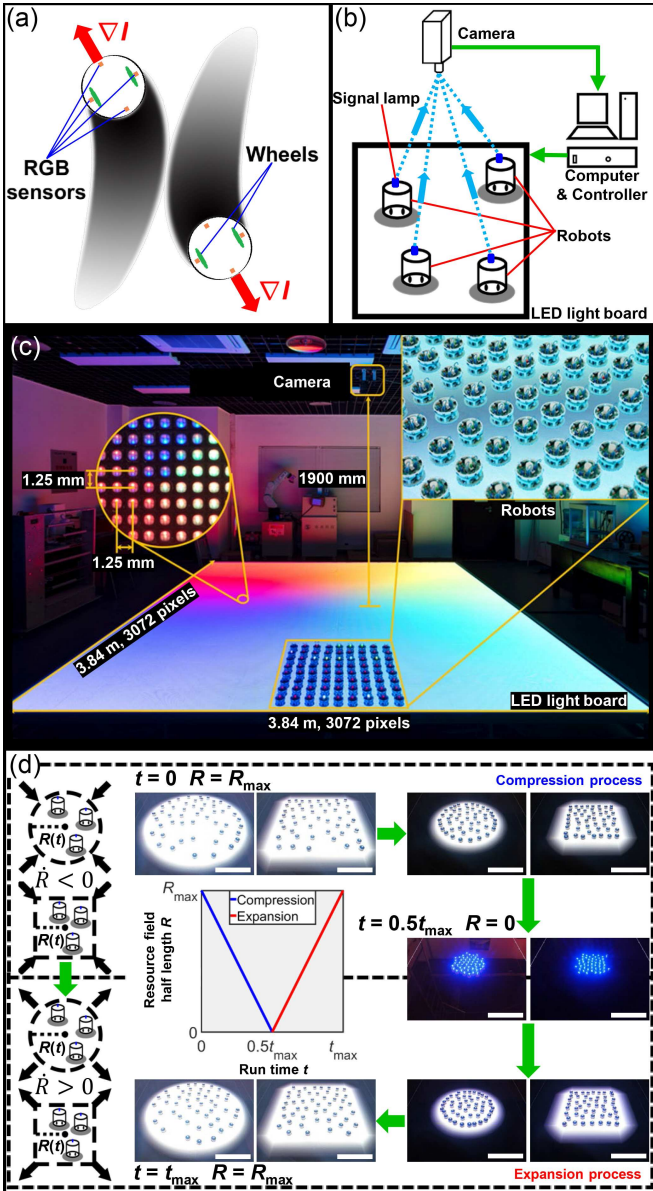


Fig. 1. Schematic diagram for the experimental principle, setup, and procedure. (a) Every robot can sense the intensity of light from the underneath LED light board by four symmetrically cross-distributed RGB sensors, calculate the light gradient vectors in two mutually vertical directions by a processor, and then move to seek maximum light intensity by a two-wheel-independent drive system. Meanwhile, the local intensity of light under each robot is consumed according to the predetermined robot-environment interaction rules, and gradually recovers to its original level after the robot goes away. (b) The whole experimental platform is composed of a bottom LED light board, dozens of robots moving on the LED light board, an overhead IR CCD camera, and a corresponding computer control system. According to the signal lamps' positions captured by the camera, the local intensity of light under each corresponding robot can be adjusted to a required value. (c) The real experimental platform. (d) In a single experiment, a circular or square white light resource landscape shrinks during the first half of the time, which means the half-length of the resource field decreases linearly with time to zero. Then the resource field turns to expand, *i.e.*, its half-length increases linearly with time until it returns to the original size. Scale bar = 0.5 m.

robot swarm active matter system, the environmental compression or expansion can be achieved by decreasing or increasing the half-length R of the light resource landscape. In order to answer the question whether this robot swarm system breaks time-reversal symmetry, in a single experiment the light re-

source landscape first shrank to zero, followed by a temporally symmetrical expansion. In other words, as shown in Fig. 1(d), the half-length $R(t)$ decreased linearly with time t to zero during the first half of the time, and then increased linearly with time t to the original size R_{\max} :

$$\begin{cases} R(t) = R_{\max} - \alpha t, & \text{when } t \leq 0.5t_{\max}, \\ R(t) = \alpha t - R_{\max}, & \text{when } t > 0.5t_{\max}, \end{cases} \quad (4)$$

where α is the change rate of the half-length R and $t_{\max} = 2R_{\max}/\alpha$. For simplicity, the initial color of the light resource landscape was set as white ($I_{\text{Red}} = I_{\text{Green}} = I_{\text{Blue}} = 255$). To study the effect of the boundary geometry of the light resource landscape, we used the circular boundary condition and the square boundary condition to make a comparison analysis. To keep the robots moving in the white light landscape, it is necessary to provide gradients at the boundary, and thus the boundary was softened by a fixed Gaussian width $\sigma_b \ll R_{\max}$. In this study, 49 robots were randomly put into the white light environment, the robotic motion sensitivity $\kappa \approx 0.03 \text{ mm}^2/\text{ms}/\text{lightintensity}$, the robotic characteristic resource consumption rate $k_c = 14 \text{ light-intensity}/\text{timestep}$, the robotic characteristic resource consumption radius $\sigma = 65 \text{ mm}$, the original half-length $R_{\max} = 875 \text{ mm}$, and the half-length change rate $\alpha \approx 0.83 \text{ mm/s}$.

In the process of changing swarm density, the spatial distribution and motive degree of the robots keep changing as well, so appropriate spatial and temporal order parameters are needed to evaluate the states of the robot swarm. For spatial ordering, the m -fold orientational order parameter ψ_m which is used for estimation of the 2D crystals with m -fold rotational symmetry is a common and effective choice.^[35] Considering that the densest packing of disks in 2D is the hexagonal array^[36] and the fourfold rotational symmetry of the square boundary, ψ_6 and ψ_4 are natural choices to characterize the spatial ordering of the robots:^[37]

$$\psi_m = \left\langle \frac{1}{N_n} \sum_{j=1}^{N_n} e^{im\theta_{nj}} \right\rangle_{\text{bulk}}, \quad (5)$$

where θ_{nj} is the angle between the vector connecting the robot n to its j -th nearest neighbor and an arbitrary fixed reference axis, and N_n is the number of nearest neighbors of the robot n . $\langle \cdot \rangle_{\text{bulk}}$ means averaging over all robots excluding ones near the boundary of the landscape. Voronoi tessellation^[38] was combined with distance threshold to determine the nearness relationship between robots and to the boundary. For temporal ordering, we chose the susceptibility characteristic timescale τ^* derived from the dynamic four-point susceptibility order parameter χ_4 to characterize the average trapping time of a robot around a given position.^[39,40] To calculate χ_4 , the dynamical overlap function $Q(t, \tau; a)$ is needed to be calculated

first:

$$Q(t, \tau; a) = \frac{1}{N} \sum_{n=1}^N \Theta(a - |r_n(t + \tau) - r_n(t)|), \quad (6)$$

where τ is the delay time, a is the characteristic length which is usually equal to the radius of an agent,^[41] *e.g.*, $a = 32.5$ mm in the experiments, N is the total number of robots, r_n is the position vector of robot n , and $\Theta(\zeta)$ is a Heaviside unit step function, *e.g.*, $\Theta(\zeta > 0) = 1$, $\Theta(\zeta \leq 0) = 0$. Then the function $\chi_4(\tau; a)$ can be calculated as the variance of $Q(t, \tau; a)$ over the quasi-steady-state time interval:

$$\chi_4(\tau; a) = N \times \text{Var}_t(Q(t, \tau; a)). \quad (7)$$

Finally, the susceptibility characteristic timescale τ^* can be determined from the peak position of $\chi_4(\tau; a)$.

2.3. Simulation

To make further research about the experimental phenomena, we did dynamic simulations based on the actual robotic behaviors. The computational domain was a 2D square with a size of $2 \text{ m} \times 2 \text{ m}$ and a spatial resolution of 1.25 mm , and each robot was simplified to a 2D disk with a diameter of 65 mm . The timestep of the simulation was set as 0.25 s and all other robotic and environmental parameters were the same as those in the experiments. The positions and orientations of robots were completely random at the beginning of every simulation. To reappear the symmetry-breaking starting in the experiments, when a virtual robot was stationary or moved along the gradient and the local intensity was high enough, an extra small forward intensity gradient was applied to the robot to play the role of the positive-feedback mechanisms. A speed-dependent sub-timestep segmentation and a constant-direction and symmetrical-distance collision method were applied to deal with the virtual physical collisions between robots. The analysis methods of the simulations were the same as those in the experiments.

3. Results and discussion

During the compression process of the white light resource landscape with the environment recovery rate $1/\tau_R = 0.4 \text{ timestep}^{-1}$, no matter whether under the circular boundary condition or the square boundary condition, four different collective states emerged sequentially from gas, via crystal, liquid, to jammed state, as shown in Fig. 2. This experimental phenomenon is in agreement with our previous work.^[24] In the preparing stage of every experiment, the robots were randomly placed on the white light resource landscape, so the experimental phenomenon was independent of the initial spatial distribution of the robots. At the beginning of the compression process, the density of robots was so small that only

a small number of two-body interaction events happened. In this scenario, the two-body interaction event, *e.g.*, the overlapping of the shadows created by two nearby robots, provided a purely repulsive effect. Hence, the robots moved freely at most of the time and acted like an ensemble of gas particles which were dominated by random diffusion with low ψ_6 , low ψ_4 , and low τ^* , as shown in Figs. 3 and 4 which are the average results of three repeated experiments. With increasing compression, the density of robots and the number of interaction events increased as well. The gradients of the overlapped shadows steepened as the distances between two nearby robots decreased. When the slope of the gradient between two nearby robots exceeded the maximum resource slope S_m a robot can move against, an impenetrable field barrier was generated. Since the robots have no physical inertia, a robot should freeze if it is surrounded by symmetrically distributed field barriers. Once the number of global field barriers became big enough and there was still some space for the robots to adjust their positions, the robots could freeze into a symmetrical crystalline state. As shown in Figs. 2(b1) and 2(b2), robots in the center of the swarm formed a hexagonal array under the circular boundary condition, while there was a square array in the center of the swarm when the boundary was square. Correspondingly, as shown in Figs. 3 and 4, ψ_6 was high, ψ_4 was low, and τ^* was high in the crystalline state under the circular boundary condition, while the square boundary condition corresponded to low ψ_6 , high ψ_4 , and high τ^* . The origin of these differences came from that the outmost robots needed to adapt themselves to the environmental boundary and this effect could spread across the whole swarm as the density was big enough. Therefore, the spatial structure of the robots in the crystalline state has a high dependence on the shape of the environmental boundary, which means the type of the main characteristic spatial order parameter of the swarm is determined by the geometry of the boundary.

With the further decreasing of resource landscape area and the further increasing of robot density, the overlap degree of the consumed shadows increased, so the global average resource intensity and the roughness of resource landscape both decreased. Hence, the slopes of the gradients between any two nearby robots became small again, and the number of impenetrable field barriers decreased. Meanwhile, the physical impenetrable barriers of the robots themselves began to influence the motion of the swarm. The conversion of the barrier type brought the decrease of the width of the impenetrable barriers, so the robots with the ability of the counter-gradient motion had the chances to escape from the lattice positions and move freely in a small range. At the swarm level, the crystal state gradually melted into a liquid state with a decrease in ψ_6 , ψ_4 , and τ^* , as shown in Figs. 3 and 4. Finally, as the swarm

was compressed to its limit when the robots physically contact with each other and the whole environment became black, the swarm reached a jammed state with high ψ_6 , low ψ_4 , and high τ^* .

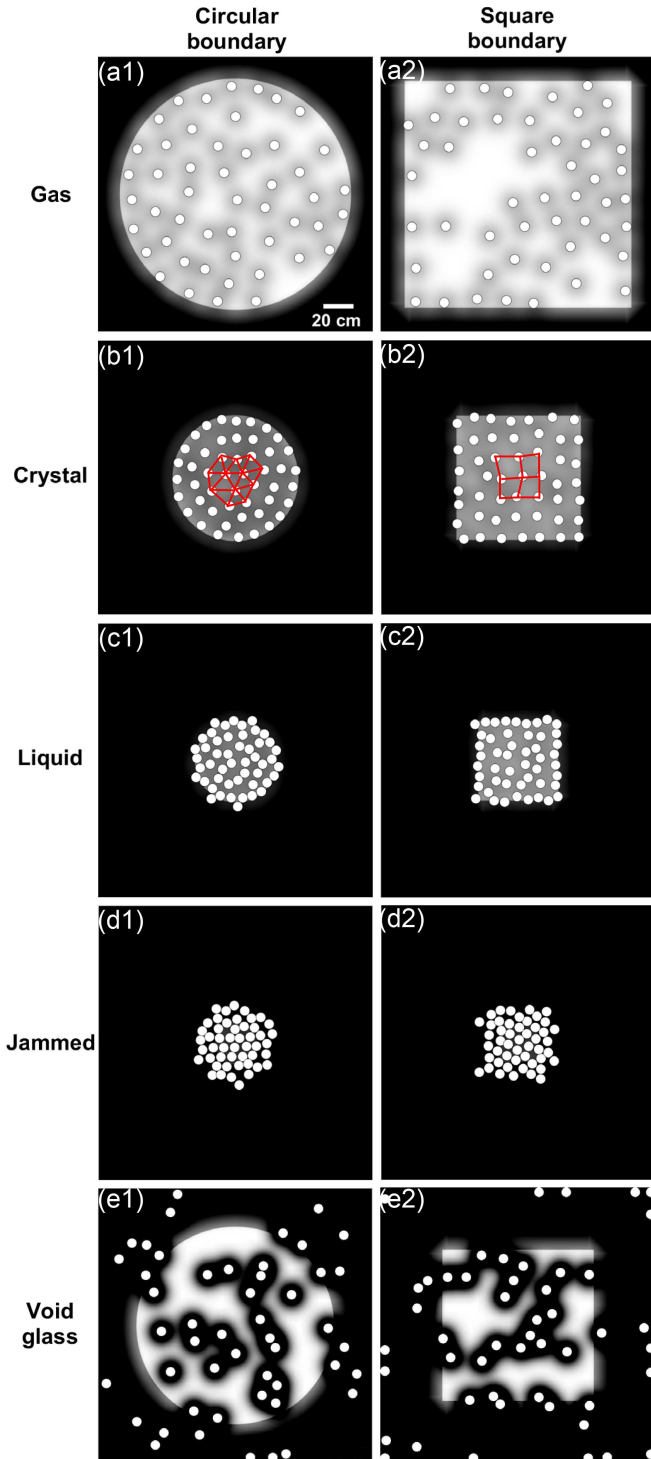


Fig. 2. Comparison of the typical robot spatial distribution states in the experiment as the white light resource landscape shrinks between in circular boundary condition and square boundary condition. Column (a1)–(e1) shows snapshots of robot positions in gas, crystal, liquid, jammed, and void glass states in circular boundary condition, and column (a2)–(e2) corresponds to square boundary condition. The red lines in panel (b1) show that the robots emerge into a hexagonal crystalline state in circular boundary condition, while the red lines in panel (b2) point to a square crystalline state in square boundary condition.

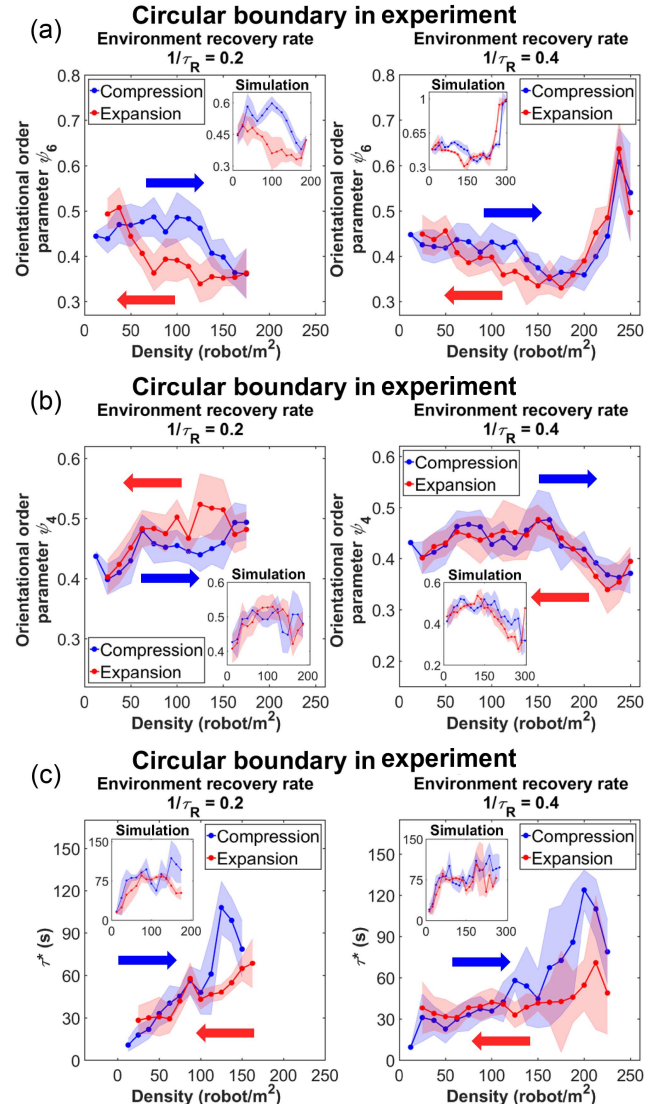


Fig. 3. The spatial and temporal ordering dynamic of the robot swarm as the circular white light resource landscape shrinks and expands in the experiment when environment recovery rate $1/\tau_R = 0.2$ time step⁻¹ and $1/\tau_R = 0.4$ time step⁻¹. The insets show the corresponding simulation results. The shadow regions represent error bars. (a) The sixfold orientational order parameter ψ_6 for hexagonal spatial ordering. (b) The fourfold orientational order parameter ψ_4 for square spatial ordering. (c) The susceptibility characteristic timescale τ^* for the mean residence time of a robot around a given position.

The environmental recovery rate $1/\tau_R$ is a key parameter in this system, because it can affect the final spatial phase reached by the swarm in the compression process and the degree of spatial symmetry in the crystal state. With a too small environmental recovery rate, the whole light resource environment is quickly consumed to all black by the robots at a swarm density which is far smaller than the density of the jammed state, and then the robots all freeze to a void glass state because the robots have no physical inertia, as shown in Figs. 2(e1) and 2(e2). This glass transition can happen at any moment determined by the value of the environmental recovery rate during the compression process, which means gas, crystal and liquid states all can directly transit to the void glass state. The smaller the environmental recovery rate is, the ear-

lier the swarm gets into the void glass state. On the other hand, in the crystal state smaller environment recovery rate leads to darker shadows which make the effect of impenetrable field barriers stronger. As the restriction strength and stability of the lattice positions improve, the order degree of the crystal state increases, so the main characteristic spatial order parameter and the susceptibility characteristic timescale both increase at the crystalline density when the environment recovery rate decreases, as shown in Figs. 3 and 4.

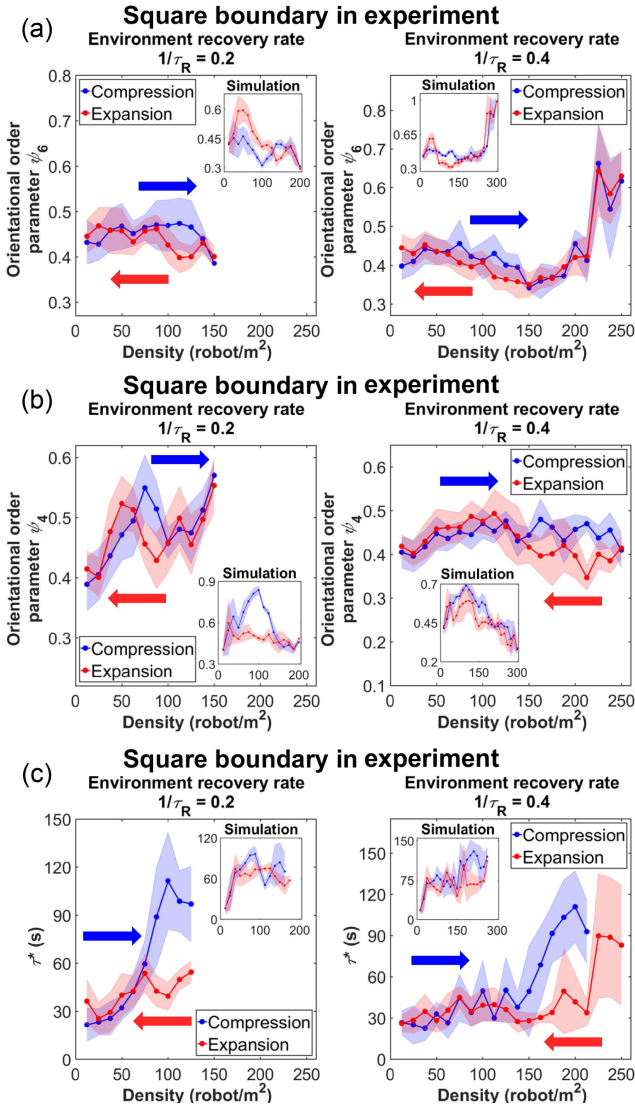


Fig. 4. The spatial and temporal ordering dynamic of the robot swarm as the square white light resource landscape shrinks and expands in the experiment when environment recovery rate $1/\tau_R = 0.2$ time step⁻¹ and $1/\tau_R = 0.4$ time step⁻¹. The insets show the corresponding simulation results. The shadow regions represent error bars. (a) The sixfold orientational order parameter ψ_6 for hexagonal spatial ordering. (b) The fourfold orientational order parameter ψ_4 for square spatial ordering. (c) The susceptibility characteristic timescale τ^* for the mean residence time of a robot around a given position.

During the expansion process of the white light resource landscape from the jammed swarm state, the spatial disorder, and motive degree of the robots significantly increased within a certain density range compared to the compression process, as shown in Figs. 3 and 4. These differences between the com-

pression process and the expansion process were more significant in the main characteristic spatial order parameter relevant to the boundary condition when the environment recovery rate was smaller, because the spatial symmetry and stability of the crystal state in the compression process increased under such conditions. Because the initial positions of the robots were determined by randomly manual placement before the compression process while the final positions of the robots were the results of swarm evolution at the end of the expansion process, the distances between the outmost robots and the environmental boundary at the beginning of the compression process could be shorter than that at the end of the expansion process. Hence, the minimum density of the compression process could be smaller than the minimum density of the expansion process, as shown in Fig. 3. In summary, in the expansion stage the crystal state almost vanished and the density range of the liquid state significantly increased. Hence, the time-reversal symmetry was broken in the compression–expansion process of the robot swarm with this two environment recovery rates.

Considering the experimental limitations such as the robotic battery life and so on, we did dynamic simulations to make further research about this time-reversal symmetry-breaking phenomenon, and the corresponding simulation results are shown in the insets of Figs. 3 and 4. The simulation results almost captured all the qualitative characteristics and evolutionary processes of the experimental swarm system, and they are closer to the predictions of the phenomenological theory earlier in this article. The consistency between the experimental results and the simulation results comes from the directness of the interaction rules based on the resource field without flowability in this study. The experimental results and the simulation results confirmed with each other, so the conclusion of this study should be more reliable. The differences between the experimental results and the simulation results may come from the electronic noise and heterogeneity in the robots, the errors in the corresponding relationship between the coordinates of the light board and the coordinates of the camera, and other experimental errors. Further, we did simulations of the first compression stage, the first expansion stage and the second compression stage with a series of environment rates for comprehensive analysis and research, as shown in Figs. 5 and 6 which are the average results of three repeated simulations. Compared to the first compression stage, there was a significant drop of τ^* in the first expansion stage, which means the fluidity of the swarm increased. Furthermore, a more disorderly spatial distribution of the first expansion stage was reflected in ψ_6 under the circular boundary condition or ψ_4 under the square boundary condition, which appeared as that the liquid region swallowed up the crystal region. So, the simulation results further confirmed the time-reversal symmetry-breaking evolution of the swarm during the compression–expansion process. On the other hand,

the high similarity between the first compression stage and the second compression stage indicated that the spatial-temporal evolution process of the swarm was cyclical when a whole compression–expansion process was regarded as a cycle. Intuitively, the dynamic loop of the main characteristic spatial order parameter with swarm density is very similar to the magnetic hysteresis loop,^[42] and thus this phenomenon may be called orderly hysteresis.

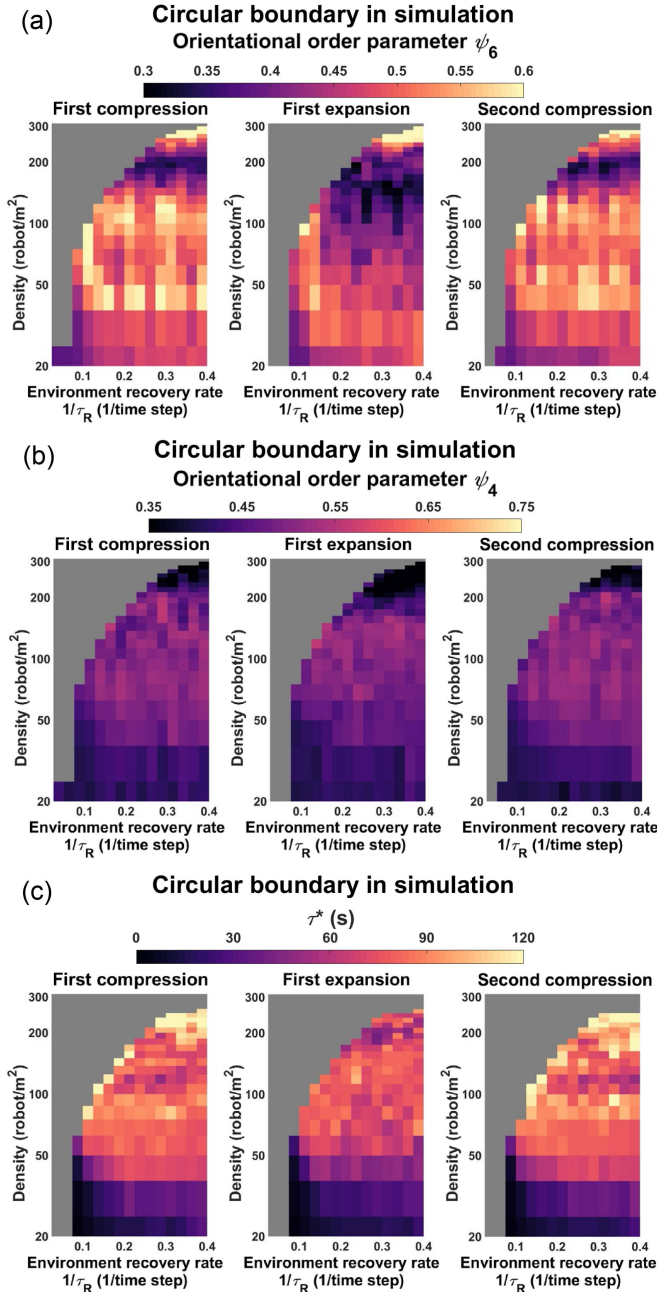


Fig. 5. The phase evolution process of the robot swarm in the compression–expansion cycle of the circular white light resource landscape of a variety of environment recovery rate in simulation, *i.e.*, the order parameters as a function of robot density and environment recovery rate in the first compression process, the first expansion process, and the second compression process of circular environment. (a) The sixfold orientational order parameter ψ_6 . The grey areas represent the void glass state. (b) The fourfold orientational order parameter ψ_4 . The grey areas represent the void glass state. (c) The susceptibility characteristic timescale τ^* . The grey areas represent $\tau^* \rightarrow \infty$.

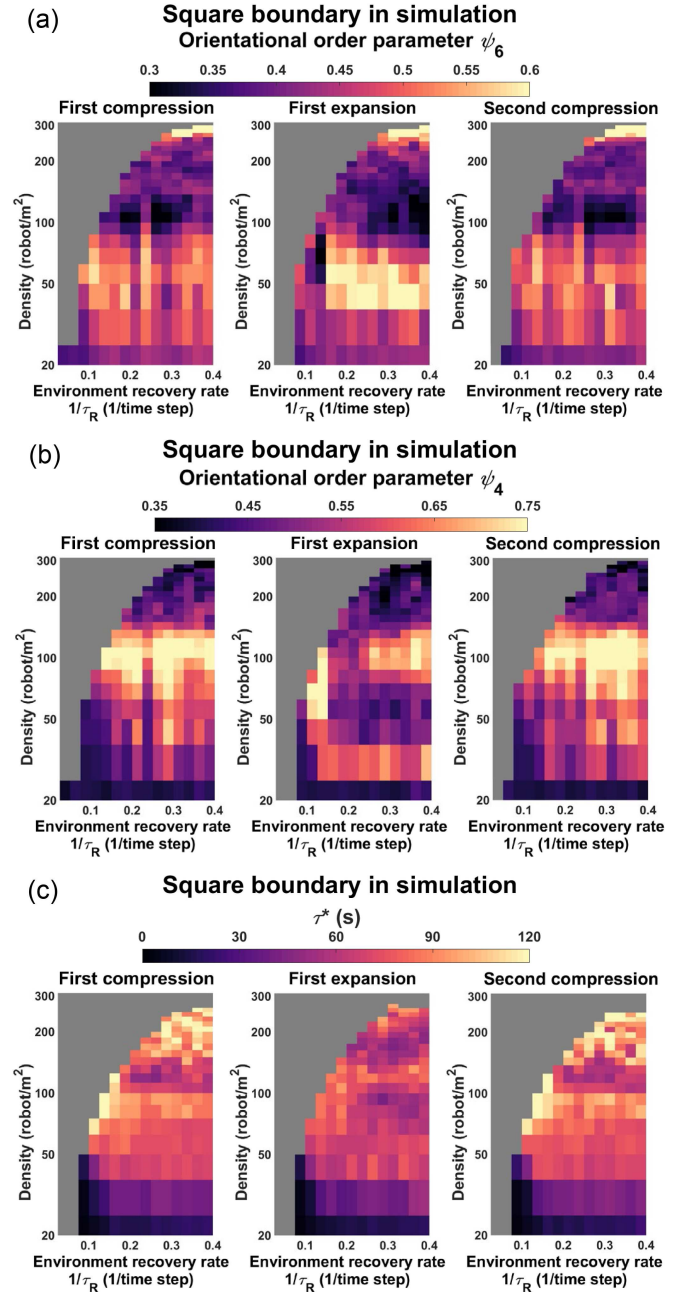


Fig. 6. The phase evolution process of the robot swarm in the compression–expansion cycle of the square white light resource landscape of a variety of environment recovery rate in simulation, *i.e.*, the order parameters as a function of robot density and environment recovery rate in the first compression process, the first expansion process, and the second compression process of square environment. (a) The sixfold orientational order parameter ψ_6 . The grey areas represent the void glass state. (b) The fourfold orientational order parameter ψ_4 . The grey areas represent the void glass state. (c) The susceptibility characteristic timescale τ^* . The grey areas represent $\tau^* \rightarrow \infty$.

As the appearance of magnetic hysteresis is due to the energy barriers in the irreversible growth of domains with the orientation of the magnetic moments parallel to the applied magnetic field,^[42] the orderly hysteresis may come from the irreversible motion caused by impenetrable barriers. The robots have nearly total freedom to move in the whole white light resource landscape at the gas density, so there is basically no irreversible motion at this phase. With the continued increase

of swarm density, impenetrable field barriers begin to emerge, then grow in number, and finally are replaced by impenetrable physical barriers. Meanwhile, the global resource substantially decreases, so the motion type of robots gradually changes from reversible motion to irreversible motion. Hence, in the expansion process only if the swarm density comes close to the gas density, do the robots have a chance to adjust their positions in a large scale. That is why there is a narrow peak of the main characteristic spatial order parameter in the transition region between the liquid state and the gas state during the expansion process. Viewed from another perspective, considering that the kinetic energy of the robots is in contrary relation to τ^* , the mobility of the robots is stronger when they reach the crystal density from the gas density in the compression stage than that when they reach the crystal density from the liquid density in the expansion stage. Hence, the search efficiency for appropriate lattice positions is higher in the compression stage, which leads to a higher probability of a good lattice structure. Furthermore, a theory from the aspect of force balance may also partly explain this phenomenon. In the compression stage, the contraction of the environment provides a force which decreases the distances between the robots, while the repulsive effect from the resource competition plays a role as a force increasing the distances between the robots. So, force-balanced lattice positions could be generated with these two opposite forces. On the other hand, the dilatation of the environment and the resource competition both increase the distances between the robots in the expansion stage, and thus there is nearly no appropriate spacing for the robots to stop. In addition, the key environmental parameters had significant influence on the orderly hysteresis loop. Since a too small environment recovery rate or a too fast environmental half-length change rate makes the swarm transit into the void glass state at a smaller density, the decrease of the environment recovery rate or the increase of the environmental half-length change rate turns the loop into an incomplete form like the unsaturated magnetic hysteresis loop. But unlike the reduce of the area of the unsaturated magnetic hysteresis loop, the areas of close curves with smaller environment recovery rates are bigger than those of complete loops because of the order enhancement property of small environment recovery rates, as shown in Figs. 3 and 4. Although the simulation results displayed comprehensively the physical phenomena of the positional order of the robot swarm in this study, once more complicated physical mechanisms, such as many-body physical collision, spin, and the interaction between actuators, are introduced and more dynamic physical phenomena, such as the orientational order and the mechanical property of the swarm, are focused, the difficulty of modeling and the computing time of simulation will increase sharply, so the experimental data will provide an accurate representation of the physical phenomenon in a much more efficient and comprehensive manner.

4. Conclusion

In the environmental compression–expansion cycle, our robot swarm demonstrates a good adaptability to the environmental influence, especially to the environmental boundary geometry. The order enhancement property of small environment recovery rates correlates with the enhanced perceptual capability of organisms in a harsh environment. Due to the complex interaction between the robots and between each robot and the environment, a time-reversal symmetry-breaking orderly hysteresis emerges. These results present many similarities between the ecosystems with resource consumption on a long-time scale and the physical systems with energy dissipation on a short-time scale,^[12,43–46] suggesting that the irreversible energy-consuming nature of active matter can lead to many similar phenomena in systems with different scales, and different mechanisms.

Acknowledgments

Project supported by the National Natural Science Foundation of China (Grant Nos. 11974066 and 12174041) and the Seed Grants from the Wenzhou Institute, University of Chinese Academy of Sciences (Grant No. WIUCASQD2021002).

References

- [1] Fodor É, Nardini C, Cates M E, Tailleur J, Visco P and Van Wijland F 2016 *Phys. Rev. Lett.* **117** 038103
- [2] Ramaswamy S 2017 *J. Stat. Mech.* **2017** 054002
- [3] Needleman D and Dogic Z 2017 *Nat. Rev. Mater.* **2** 17048
- [4] Fang X, Kruse K, Lu T and Wang J 2019 *Rev. Mod. Phys.* **91** 045004
- [5] Wang Y X and Chen S 2015 *Acta Phys. Sin.* **64** 054701 (in Chinese)
- [6] Zhang H P, Shi X Q and Yang M C 2022 *Physics* **51** 217 (in Chinese)
- [7] Marchetti M C, Joanny J F, Ramaswamy S, Liverpool T B, Prost J, Rao M and Simha R A 2013 *Rev. Mod. Phys.* **85** 1143
- [8] Mahault B, Jiang X C, Bertin E, Ma Y Q, Patelli A, Shi X Q and Chaté H 2018 *Phys. Rev. Lett.* **120** 258002
- [9] Mahault B and Chaté H 2021 *Phys. Rev. Lett.* **127** 048003
- [10] Vicsek T and Zafeiris A 2012 *Phys. Rep.* **517** 71
- [11] Giomi L 2015 *Phys. Rev. X* **5** 031003
- [12] Nguyen N H P, Klotsa D, Engel M and Glotzer S C 2014 *Phys. Rev. Lett.* **112** 075701
- [13] Liao G J and Klapp S H L 2021 *Soft Matter* **17** 6833
- [14] Chepizhko O, Altmann E G and Peruani F 2013 *Phys. Rev. Lett.* **110** 238101
- [15] Roy S, Shirazi M J, Jantzen B and Abaid N 2019 *Phys. Rev. E* **100** 062415
- [16] Aguilar J, Zhang T, Qian F, Kingsbury M, Mcinroe B, Mazouchova N, Li C, Maladen R, Gong C, Travers M, Hatton R L, Choset H, Umbanhowar P B and Goldman D I 2016 *Rep. Prog. Phys.* **79** 110001
- [17] Li S, Ozkan-Aydin Y, Xiao C, Small G, Gynai H N, Li G, Rieser J M, Laguna P and Goldman D I 2022 *Proc. Natl. Acad. Sci. USA* **119** e2113912119
- [18] Fruchart M, Hanai R, Littlewood P B and Vitelli V 2021 *Nature* **592** 363
- [19] Webb B 2001 *Behav. Brain Sci.* **24** 1033
- [20] Oh H, Ramezan Shirazi A, Sun C and Jin Y 2017 *Rob. Auton. Syst.* **91** 83
- [21] Slavkov I, Carrillo-Zapata D, Carranza N, Diego X, Jansson F, Kaandorp J, Hauert S and Sharpe J 2018 *Sci. Robot.* **3** eaau9178
- [22] Romano D, Donati E, Benelli G and Stefanini C 2019 *Biol. Cybern.* **113** 201
- [23] Wang G, Phan T V, Li S, Wang J, Peng Y, Chen G, Qu J, Goldman D I, Levin S A, Pienta K, Amend S, Austin R H and Liu L 2022 *Proc. Natl. Acad. Sci. USA* **119** e2120019119

- [24] Wang G, Phan T V, Li S, Wombacher M, Qu J, Peng Y, Chen G, Goldman D I, Levin S A, Austin R H and Liu L 2021 *Phys. Rev. Lett.* **126** 108002
- [25] Huber L, Suzuki R, Krüger T, Frey E and Bausch A R 2018 *Science* **361** 255
- [26] Berthier L and Kurchan J 2013 *Nat. Phys.* **9** 310
- [27] Wu K T, Hishamunda J B, Chen D T N, Decamp S J, Chang Y W, Fernández-Nieves A, Fraden S and Dogic Z 2017 *Science* **355** eaal1979
- [28] Yang Q, Zhu H, Liu P, Liu R, Shi Q, Chen K, Zheng N, Ye F and Yang M 2021 *Phys. Rev. Lett.* **126** 198001
- [29] Wu C, Dai J, Li X, Gao L, Wang J, Liu J, Zheng J, Zhan X, Chen J, Cheng X, Yang M and Tang J 2021 *Nat. Nanotechnol.* **16** 288
- [30] Bowick M J, Fakhri N, Marchetti M C and Ramaswamy S 2022 *Phys. Rev. X* **12** 010501
- [31] Ro S, Guo B, Shih A, Phan T V, Austin R H, Levine D, Chaikin P M and Martiniani S 2022 *Phys. Rev. Lett.* **129** 220601
- [32] Liu S, Shankar S, Marchetti M C and Wu Y 2021 *Nature* **590** 80
- [33] Phan T V, Wang G, Liu L and Austin R H 2021 *Symmetry* **13** 225
- [34] Saha T and Galic M 2018 *Phil. Trans. R. Soc. B* **373** 20170113
- [35] Steinhardt P J, Nelson D R and Ronchetti M 1983 *Phys. Rev. B* **28** 784
- [36] Atkinson S, Stillinger F H and Torquato S 2014 *Proc. Natl. Acad. Sci. USA* **111** 18436
- [37] Eslami H, Sedaghat P and Müller-Plathe F 2018 *Phys. Chem. Chem. Phys.* **20** 27059
- [38] Debnath D, Gainer J S, Kilic C, Kim D, Matchev K T and Yang Y P 2016 *Eur. Phys. J. C* **76** 645
- [39] Reisz T 1995 *Nucl. Phys. B* **450** 569
- [40] Godina J J, Meurice Y, Oktay M B and Niermann S 1998 *Phys. Rev. D* **57** 6326
- [41] Keys A S, Abate A R, Glotzer S C and Durian D J 2007 *Nat. Phys.* **3** 260
- [42] Gatteschi D, Sessoli R and Villain J 2006 *Molecular Nanomagnets* (Oxford: Oxford University Press on Demand) p. 60
- [43] Petroff A P, Wu X L and Libchaber A 2015 *Phys. Rev. Lett.* **114** 158102
- [44] Tan T H, Mietke A, Li J, Chen Y, Higinbotham H, Foster P J, Gokhale S, Dunkel J and Fakhri N 2022 *Nature* **607** 287
- [45] Getzin S, Holch S, Yizhaq H and Wiegand K 2022 *Perspect. Plant Ecol. Evol. Syst.* **57** 125698
- [46] O'byrne J, Kafri Y, Tailleur J and Van Wijland F 2022 *Nat. Rev. Phys.* **4** 167